PNAS RESEARCH ARTICLE | MEDICAL SCIENCES

Mitochondrial double-stranded RNA fuels pancreatic cancer growth via RIG-I/TLR3 inflammation

Andrew T. Milcarek[a,1], Minjeong Yeon[a,1,2], Camilla Esposito[a,b], Prerna Kulkarni[a], Andrew V. Kossenkov[a,c], Jozef Madzo[a,c], Anneliese M. Faustino[d], Hsin-Yao Tang[d,e], Alessandra M. Storaci[f], Alessandro Palleschi[g,h], Marco Locatelli[h,i], Valentina Vaira[f,g], Mary V. Iacocca[j,k], Andrea Ward[j,k], Arvind Sabesan[k,l], Nicholas J. Petrelli[k], Michela Perego[a,3], and Dario C. Altieri[a,3]

Affiliations are included on p. 8.

Edited by John Hiscott, Istituto Pasteur-Fondazione Cenci Bolognetti, Rome, Italy; received October 8, 2025; accepted March 16, 2026 by Editorial Board Member Kornelia Polyak

Mitochondria activate inflammation and innate immunity to protect against infections, but the role in cancer is unknown. Here, we report that patients with pancreatic ductal adenocarcinoma (PDAC) with reduced levels of the mitochondrial scaffold, Mic60, or inner mitochondrial membrane protein, exhibit increased inflammation, high NFκB activity and production of TNFα. This is mediated by double-stranded RNA (dsRNA) released from structurally defective, Mic60-low mitochondria, which engages TLR3/RIG-I sensing, activates NFκB gene expression and reprograms transcriptional and signaling networks to promote PDAC proliferation. Preclinical targeting of mitochondrial dsRNA signaling triggers rapid cell death and inhibition of tumor growth, selectively in Mic60-knockdown PDAC, without overt toxicity, in vivo. Therefore, dsRNA released from defective mitochondria generates protumorigenic inflammation and provides an actionable therapeutic target in selected PDAC patients.

pancreatic cancer | dsRNA | viral mimicry | TLR3 | inflammation

Significance

Pancreatic ductal adenocarcinoma (PDAC) is a major unmet medical need: The standard of care for these patients has not changed in decades, life expectancy is abysmal, and more effective therapies are yet to be discovered. We now find that PDAC patients harbor structurally defective mitochondria due to reduced levels of the scaffold protein, Mic60. In turn, this causes the release of mitochondrial double-stranded RNA (dsRNA) in cytosol, a potent viral-like stimulus that activates inflammation, reprograms transcriptional networks, and fuels PDAC proliferation. This pathway of mitochondrial inflammation exposes an actionable therapeutic vulnerability, and targeting dsRNA signaling suppresses PDAC growth without overt toxicity in preclinical models.

In addition to bioenergetics, redox balance, and interorganelle communication, mitochondria are signaling hubs of innate immunity and inflammation (1, 2). This protects against invading pathogens (3), mostly viruses, as a host of molecules deputed to sense foreign nucleic acids engage the mitochondrial antiviral signaling protein (MAVS) (4) and transduce an inflammatory response with high nuclear factor-κB (NFκB) gene expression (5), upregulation of type I and III interferons (IFN) (6) and release of pleiotropic cytokines/chemokines.

Mislocalized or aberrantly processed *endogenous* nucleic acids are also detected by the same sensing machinery to trigger inflammation (7). Described as "viral mimicry," this process has been linked to altered epigenetics (8, 9), chromosomal missegregation (10), or aberrant RNA splicing (11), culminating with the reactivation of endogenous retroviruses in the nuclear genome (12). There is evidence that endogenous DNA (13) or RNA (14), including double-stranded RNA (dsRNA) released by damaged or "stressed" mitochondria can also mimic viral nucleic acids (15), activate sensor mechanisms, and fuel inflammation. This process of mitochondrial viral mimicry has been linked to disease pathogenesis and cellular senescence (16, 17), but its role in cancer, where mitochondrial stress and loss of organelle integrity are common (18), has not been explored.

A key regulator of mitochondrial integrity is the scaffold molecule, Mic60, or inner mitochondrial membrane protein (IMMT). This is a component of the mitochondrial contact site and cristae organizing system (MICOS) complex that maintains cristae architecture, assembly of respiratory complexes and membrane biogenesis (19). Despite these essential functions, Mic60 levels are heterogeneous and even undetectable in many human tumors, resulting in structurally defective and dysfunctional mitochondria (20). In turn, Mic60-knockdown mitochondria become hubs of cellular "stress" signals (20), including an inflammatory gene signature that correlates with aggressive disease variants and treatment resistance in patients with pancreatic ductal adenocarcinoma (PDAC) (21).

Despite considerable efforts, PDAC remains one of the deadliest cancer diagnoses, in acute need of new, actionable therapeutic targets (22). We know that widespread inflammation through increased NFκB gene expression is linked to poor outcome (23), but the underlying mechanisms and potential therapeutic vulnerabilities remain elusive.

Results and Discussion

NFκB Inflammation in PDAC. To determine how Mic60 levels affect PDAC inflammation (21), we first examined RNA-seq datasets in TCGA. Here, PDAC patients with low expression of Mic60 exhibited a gene signature of acute inflammation, angiogenesis,

The authors declare no competing interest.

This article is a PNAS Direct Submission. J.H. is a guest editor invited by the Editorial Board.

[1]A.T.M. and M.Y. contributed equally to this work.

[2]Present address: Department of Biochemistry, Chungbuk National University College of Medicine, Cheongju 28160, Republic of Korea.

[3]To whom correspondence may be addressed. Email: mperego@wistar.org or daltieri@wistar.org.

This article contains supporting information online at https://www.pnas.org/lookup/suppl/doi:10.1073/pnas.2528281123/-/DCSupplemental.

Published April 28, 2026.

and cytokine release (*SI Appendix*, Fig. S1 *A* and *B*), marked by heightened NFκB activity and TNFα signaling (*SI Appendix*, Fig. S1*C*). Similar results were obtained in PDAC patients stratified for high NFκB gene expression, who also showed increased inflammation and TNFα activity (*SI Appendix*, Fig. S1*D*).

To validate these findings, we next silenced endogenous Mic60 in PDAC cell lines using published protocols (20). Mic60 depletion increased the expression of multiple NFκB target genes implicated in inflammation and innate immunity (Fig. 1*A*). This was accompanied by increased NFκB promoter activity (Fig. 1*B*), upregulation of p50 and p65 NFκB subunits (Fig. 1*C*), and accumulation of p65 NFκB in the nucleus of Mic60-knockdown cells, compared to control (Fig. 1*D*). In addition, the NFκB gene signature upregulated in Mic60-knockdown PDAC cells (Fig. 1*A*) correlated with shortened overall survival in the TCGA cohort of PDAC patients (*SI Appendix*, Fig. S1*E*).

Many NFκB target genes are released extracellularly to reprogram the inflammatory microenvironment, including in cancer. To examine this possibility, we profiled the secretome released by Mic60-knockdown PDAC cells by mass spectrometry. Consistent with the data above, PDAC cells with reduced expression of Mic60 released high levels of TNFα in the conditioned medium (siMic60 vs. siCtrl, ↑1,314-fold, adjusted $P = 6.1 \times 10^{-7}$) (Fig. 1*E*). Similar results were obtained by ELISA, where TNFα levels increased from 0.17 ± 0.06 pg/mL in the conditioned medium of control cells to 354 ± 17.7 pg/mL after Mic60 depletion (*SI Appendix*, Fig. S1*F*). Mediators of redox balance and inflammation were also differentially upregulated in the Mic60-knockdown secretome (TXN, ↑3.4-fold, adjusted $P = 0.003$; PRDX1, ↑2.9-fold, adjusted $P = 0.0006$; NQO2, ↑6.6-fold, adjusted $P = 0.0004$; NQO1, ↑4.1-fold, P.adj = 0.003), whereas collagen isoforms involved in extracellular matrix reorganization and PDAC desmoplastic stroma (24) were downregulated (Fig. 1*E*).

We next studied a cohort of 10 patients with histologically confirmed diagnosis of PDAC (*SI Appendix*, Table S1). By immunohistochemistry (IHC), Mic60 expression was uniformly strong in normal pancreatic glands (3+ IHC score) (Fig. 1*F*), but highly heterogenous with moderate (2+ IHC score) to weak (1+ IHC score) staining in PDAC patients (*SI Appendix*, Table S1 and Fig. S2). Occasional tumor areas were entirely devoid of Mic60

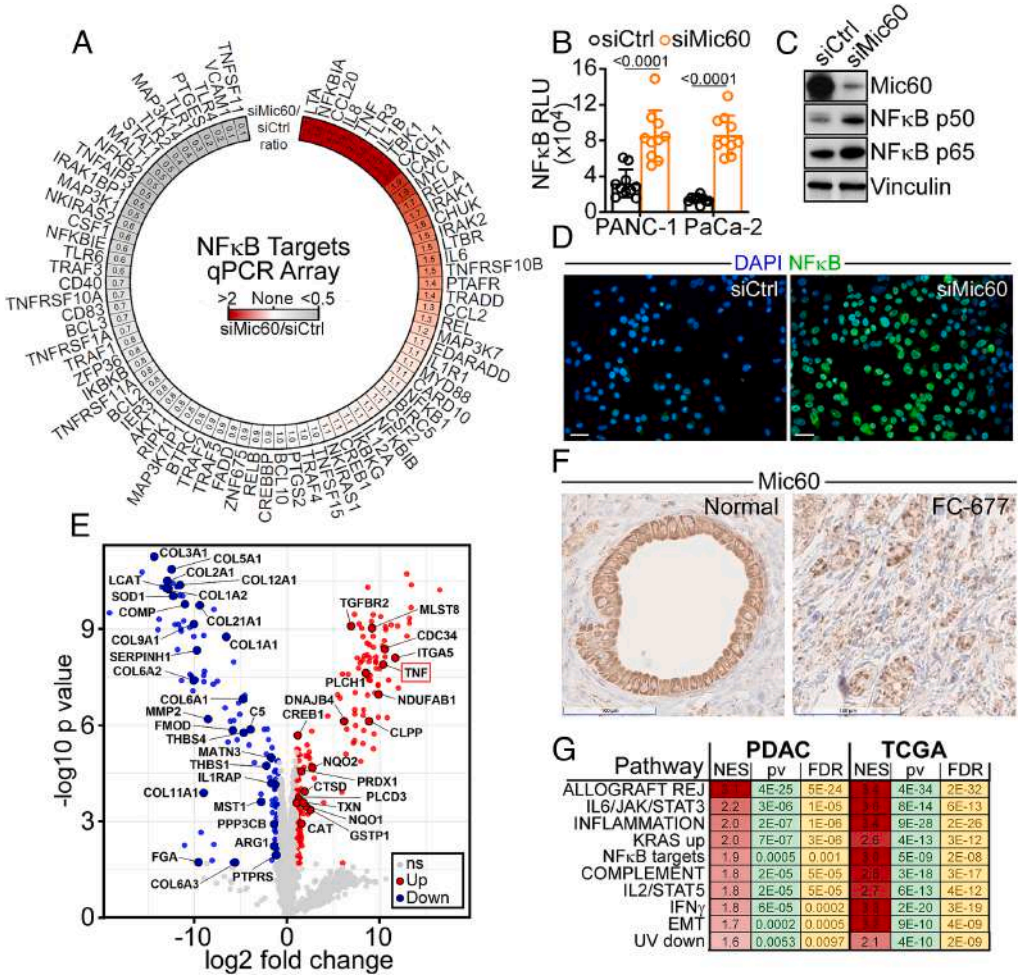

Fig. 1. NFκB inflammation in PDAC. (*A*) PANC-1 cells expressing control nontargeting siRNA (siCtrl) or Mic60-directed siRNA (siMic60) were analyzed in a 78-gene NFκB profiler array by RT-qPCR. Data are expressed as siMic60/siCtrl ratio in a radial heatmap with the ratio magnitude highlighted by color. Representative experiment. (*B*) PANC-1 or MIA PaCa-2 cells expressing siCtrl or siMic60 were analyzed for NFκB promoter reporter activity. RLU, relative luciferase units. Mean ± SD. Numbers are *P* values by two-tailed unpaired *t* test. (*C* and *D*) PANC-1 cells as in (*B*) were analyzed by Western blotting (*C*) or confocal fluorescence microscopy for nuclear localization of p65 NFκB (*D*). Representative images. (Scale bar, 20 μm.) (*E*) Aliquots of conditioned medium harvested from PANC-1 cells as in (*B*) were analyzed by mass spectrometry and 298 differentially secreted proteins were identified. Data are presented as a volcano plot showing the log2 fold change of siMic60 compared to control. TNFα released in the Mic60-knockdown *secretome* is indicated. ns, not significant. (*F*) Pancreas tissue samples from two patients with histological diagnosis of PDAC were analyzed for Mic60 expression, by immunohistochemistry. Mic60 reactivity with an adjacent normal pancreatic gland (Normal) is shown. (Scale bars, 100 μm.) (*G*) Overlap of significantly enriched hallmark pathways between eight patients with histologic diagnosis of PDAC (PDAC) and PDAC patients in the TCGA (TCGA) dataset that were significantly positively associated (FDR < 5%) with an NFκB target gene signature. For each pathway, a normalized enrichment score (NES), *P* value (pv), and false discovery rate (FDR) are indicated.

reactivity (Fig. 1*F* and *SI Appendix*, Fig. S2). We then profiled 8 of these 10 PDAC tissue samples by RNA-Seq. This revealed a strong NFκB gene signature, characterized by heightened inflammation, IFN signaling, and cytokine production (Fig. 1*G* and *SI Appendix*, Fig. S1*G*). This transcriptome matched a nearly identical gene signature upregulated in the TCGA cohort of PDAC patients (Fig. 1*G*).

dsRNA Expression in Cancer. A reduction in Mic60 levels lowers overall mitochondrial *fitness* and disrupts the organelle outer membrane (20). We hypothesized that the loss of mitochondrial integrity in these settings may cause the leakage of nucleic acids in cytosol, a potent stimulus of antiviral inflammation (1, 2). Consistent with this possibility, Mic60-knockdown PDAC cells contained abundant dsRNA in cytosol (Fig. 2*A* and *SI Appendix*, Fig. S3*A*), by fluorescence microscopy with the J2 antibody used to detect dsRNA (25). Instead, control PANC-1 cells showed no reactivity for dsRNA in cytosol (Fig. 2*A* and *SI Appendix*, Fig. S3*A*). To determine the origin of dsRNA after Mic60 depletion, we sequenced J2 immunoprecipitates from control or Mic60-knockdown PDAC cells. The immunoprecipitated dsRNA averaged ~270 nucleotides in length (*SI Appendix*, Fig. S3*B*) and its sequence aligned extensively with the mitochondrial genome (ChrM) (Fig. 2*B*). In contrast, J2 immunoprecipitates from control PDAC cells were negative (Fig. 2*B*).

Based on these data, we next asked if PDAC patients also contained dsRNA of mitochondrial origin. dsRNA immunoprecipitated from five PDAC patient samples (*SI Appendix*, Table S1)

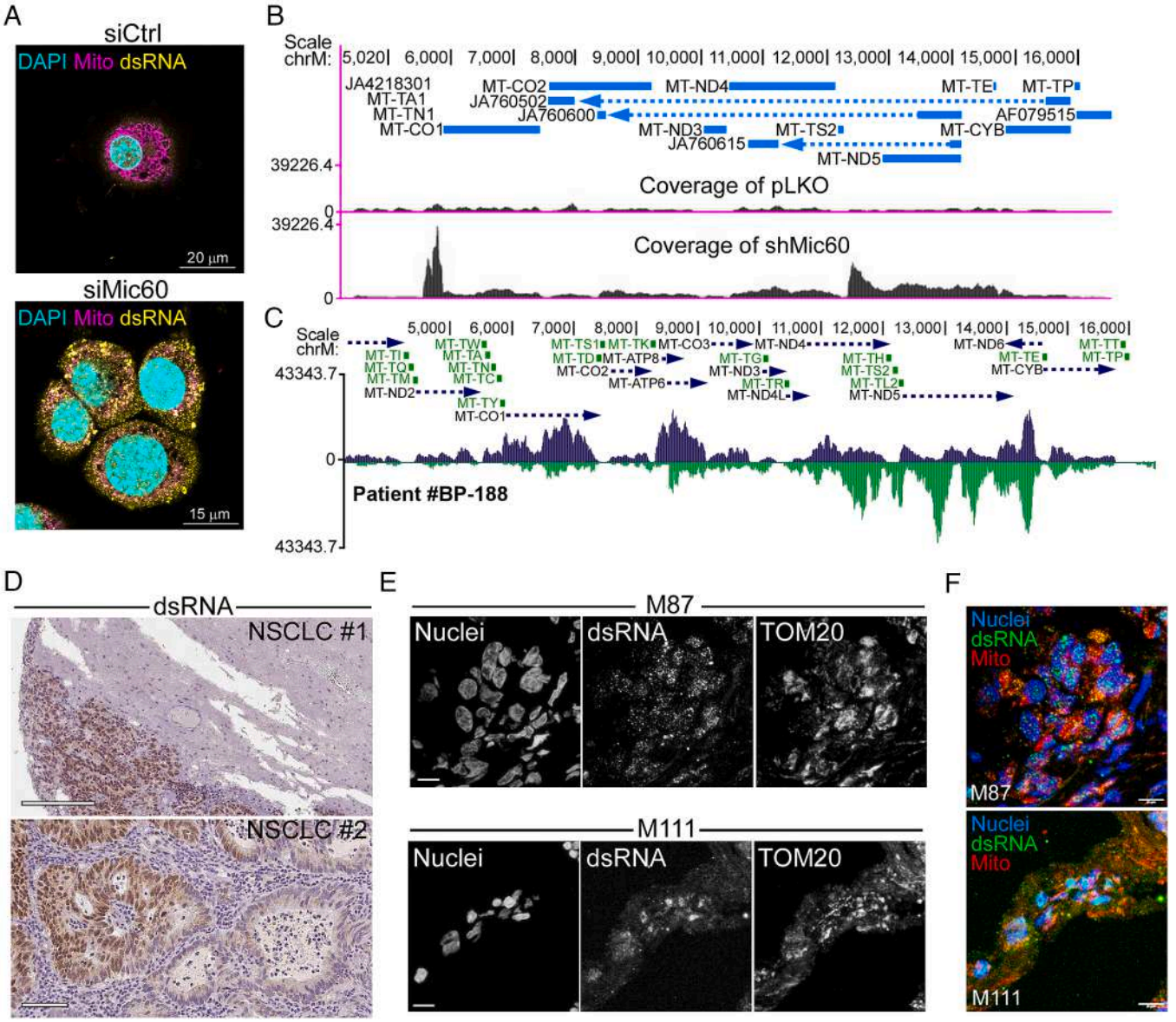

Fig. 2. Mitochondrial dsRNA in cancer. (*A*) PANC-1 cells expressing siCtrl (*Top*) or siMic60 (*Bottom*) were labeled with antibody J2 to dsRNA and analyzed by confocal fluorescence microscopy. Mitochondria and nuclei were stained with MitoTracker (Mito) and DAPI, respectively. Representative images. [Scale bars, 20 μm (*Top*) and 15 μm (*Bottom*).] (*B*) PANC-1 cells stably expressing pLKO or shMic60 were immunoprecipitated (IP) with antibody J2 and the sequence of IP dsRNA was aligned with the mitochondrial genome. The position of mitochondrial genes is indicated. (*C*) Pancreas tissue homogenates from a PDAC patient with low Mic60 expression were IP with antibody J2 and the sequence of IP dsRNA was aligned with the mitochondrial genome. The heavy (black) and light (green) strands and the position of mitochondrial genes are indicated. (*D*) Tissue samples of brain metastases from two patients with nonsmall cell lung cancer (NSCLC) were stained with antibody J2 by immunohistochemistry. Representative images. [Scale bars, 200 μm (NSCLC #1) and 70 μm (NSCLC #2).] (*E* and *F*) Snap-frozen tissue samples of surgically resected brain metastases from two patients with NSCLC (M87, M111) were stained for mitochondria (TOM20), nuclei (Hoechst), or dsRNA (J2 antibody) and analyzed by confocal fluorescence microscopy (*E*) and image merging (*F*). Representative images. (Scale bars, 10 μm.)

revealed extensive reads from the heavy and light strands of the mitochondrial genome (Fig. 2*C* and *SI Appendix*, Fig. S3*C*), suggesting that intermolecular dsRNA formed in Mic60-knockdown mitochondria escaped endogenous degradosome mechanism(s), in vivo (14). To test whether this was a unique property of PDAC, we also looked at other patient cohorts in TCGA for the presence of mitochondrial RNA. In addition to PDAC, we found that mitochondrial RNA was highly represented in multiple, unrelated tumor types, including nonsmall cell lung cancer (NSCLC) (*SI Appendix*, Fig. S3*D*). This is in line with the heterogeneous and often reduced levels of Mic60 observed in many human cancers (20).

To validate that mitochondrial dsRNA is a general trait of malignancy, we next examined tissue samples of brain metastases surgically resected from two patients with NSCLC (26), previously characterized for heterogeneous Mic60 expression, by immunohistochemistry (20). In this cohort, NSCLC brain metastases were prominently stained with the J2 antibody by IHC, whereas normal brain was negative for dsRNA (Fig. 2*D*). Tissue sections from two additional cases of NSCLC brain metastases were also J2-positive for extramitochondrial dsRNA, by immunofluorescence microscopy (Fig. 2 *E* and *F*).

dsRNA Signaling in PDAC Inflammation. To elucidate the requirements of dsRNA signaling, we first generated PANC-1 cells depleted of mitochondrial DNA by ethidium bromide treatment (ρ0 cells). As control, the expression of mitochondrial ND1 and ND4 genes, but not β-2 microglobulin (B2M) was abolished in PANC-1 ρ0 cells, compared to parental cultures, by RT-qPCR (*SI Appendix*, Fig. S4*A*). Under these conditions, Mic60 silencing stimulated NFκB promoter activity in parental PANC-1 cells, whereas PANC-1 ρ0 cells were ineffective (Fig. 3*A*). In addition, removal of dsRNA by incubation with RNAse III abolished NFκB inflammatory gene expression in Mic60-knockdown PDAC cells, compared to controls (Fig. 3*B*).

Several *sensors* of foreign or endogenous nucleic acids, including dsRNA (27), have been described that orchestrate inflammatory antiviral responses (4). We found that Mic60 silencing in PANC-1 cells prominently upregulated the expression of endosome-localized toll-like receptor 3 (TLR3) (28) as well as cytosolic retinoic acid-inducible gene I (RIG-I) (29), two key dsRNA *sensors* of antiviral signaling (Fig. 3*C*). Another cytosolic dsRNA sensor (29), melanoma differentiation-associated protein 5 (MDA5) was also upregulated by Mic60 loss, albeit less prominently (Fig. 3*C*), whereas the levels of the mitochondrial adapter MAVS (4) were comparable in control or Mic60-depleted PDAC cells (Fig. 3*C*). The TLR3-associated E3 ubiquitin ligase, TNFR-associated factor-6 (TRAF6), which is required for antiviral signaling (28) and contributes to tumor-associated inflammation (30), was also upregulated after Mic60 loss (Fig. 3*D*). This response was specific because other TRAF molecules implicated in inflammation and innate immunity; TRAF2 or TRAF3 were not affected by Mic60 levels (Fig. 3*D*). Consistent with activation of inflammatory antiviral signaling, Mic60-knockdown PANC-1 cells exhibited increased expression of Protein Kinase R (PKR) and phosphorylation of its substrate, eukaryotic translation initiation factor 2A (eIF2α) (*SI Appendix*, Fig. S4*B*), two regulators of dsRNA signaling (31).

We next examined the relative contribution of the various dsRNA sensors to NFκB activation in Mic60-knockdown PDAC cells. Here, siRNA silencing of TLR3 or TRAF6 (*SI Appendix*, Fig. S4*C*) was sufficient, independently, to suppress NFκB promoter activity induced by Mic60 depletion (Fig. 3*E*). Similar results were obtained with a small molecule inhibitor of the TRAF6–CD40 complex (TRAF6i, compound 6877002), which also suppressed NFκB promoter activity in Mic60-knockdown PANC-1 cells (Fig. 3*F*). Consistent with the data above, silencing of RIG-I (*SI Appendix*, Fig. S4*D*) prominently inhibited NFκB-directed inflammatory gene expression in Mic60-knockdown PANC-1 cells, compared to control (Fig. 3*G*). Depletion of MDA5 (*SI Appendix*, Fig. S4*D*) was less

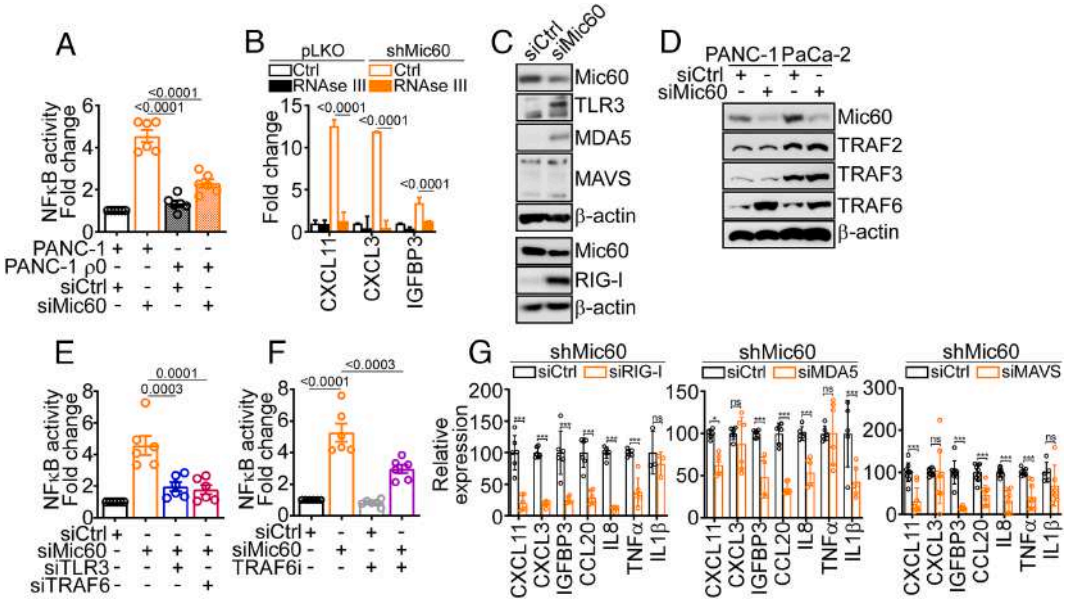

Fig. 3. Mitochondrial dsRNA signaling in PDAC. (*A*) PANC-1 cells or PANC-1 ρ0 cells depleted of mitochondrial DNA were transfected with siCtrl or siMic60 and analyzed for NFκB promoter reporter activity. Mean ± SD. (*B*) PANC-1 cells stably expressing pLKO or shMic60 were treated with RNAse III and analyzed by RT-qPCR. Mean ± SD. (*C* and *D*) PANC-1 or MIA PaCa-2 (*D*) cells expressing siCtrl or siMic60 were analyzed by Western blotting. (*E*) PANC-1 cells as in (*C*) were transfected with TRAF6 (siTRAF6)- or TLR3 (siTLR3)-directed siRNA and analyzed for NFκB promoter reporter activity. (*F*) PANC-1 cells expressing siCtrl or siMic60 were treated with a small molecule TRAF6 inhibitor (TRAF6i) and analyzed for NFκB promoter reporter activity. Mean ± SD. For panels *A*, *B*, *E*, and *F*, numbers are *P* values by two-tailed unpaired *t* test. (*G*) PANC-1 cells stably expressing shMic60 were transfected with siCtrl or siRNA to nucleic acid *sensors*, RIG-I (siRIG-I), MDA5 (siMDA5), or mitochondrial adapter protein, MAVS (siMAVS) and analyzed for normalized expression of an NFκB-dependent cytokine gene signature by RT-qPCR. Mean ± SD. The *P* values are as follows: ***, 0.0009 to 0.0001; *, 0.01; ns, not significant.

effective, and silencing of MAVS (*SI Appendix*, Fig. S4*D*) reduced the expression of most, but not all NFκB inflammatory gene products upregulated in Mic60-knockdown PANC-1 cells (Fig. 3*G*).

Specificity of Mitochondrial dsRNA Signaling in PDAC. To independently validate these results, we next carried out a proteomics screen of NFκB target proteins in control or Mic60-knockdown PANC-1 cells treated with TRAF6i. Here, small molecule TRAF6 inhibition reduced the expression of multiple NFκB inflammatory mediators, compared to control cultures (*SI Appendix*, Fig. S4*E*). This effect was specific because silencing of TLR9, a *sensor* for unmethylated CpG mitochondrial DNA (32) that activates inflammation and innate immunity (33), had no effect on nuclear accumulation of p65 NFκB (*SI Appendix*, Fig. S4*F*) or inflammatory gene expression in Mic60-knockdown PDAC cells (*SI Appendix*, Fig. S4*G*).

Next, we asked if dsRNA was the only nucleic acid released by defective Mic60-knockdown mitochondria (21). We found that Mic60 depletion modestly, albeit significantly increased the expression of mitochondria-encoded RNR2, ND1, ND2, and ND4 genes in cytosol of PANC-1 cells, compared to controls (*SI Appendix*, Fig. S5*A*). The presence of mitochondrial DNA in cytosol is predominantly *sensed* by the cyclic GMP-AMP synthase (cGAS)-stimulator of interferon genes (STING) complex, which in turn activates interferon regulatory factor 3 (IRF3)-dependent IFN and inflammatory gene expression (34). Mic60-knockdown PDAC cells exhibited only a small, ~twofold increase of 2,3-cGAMP, a second messenger in this response (*SI Appendix*, Fig. S5*B*). In addition, Mic60 depletion minimally affected the activating phosphorylation of downstream effectors of this pathway, including STING, tank binding kinase 1 (TBK1) or IRF3 (*SI Appendix*, Fig. S5*C*). Consistent with these results, siRNA silencing of STING in PANC-1 cells only partially reduced the expression of some, but not all inflammatory mediators modulated by Mic60 depletion (*SI Appendix*, Fig. S5*D*). In addition, changes in Mic60 levels did not modulate the NLR family pyrin domain-containing 3 (NLRP3) inflammasome, a host defense signaling complex activated by mitochondrial DNA (35) (*SI Appendix*, Fig. S5*E*). Together, these results suggest that mitochondrial DNA released in cytosol after Mic60 knockdown has a limited role in PDAC NFκB inflammation, compared to released dsRNA.

Reprogramming of Transcriptional Networks in Mic60-Knockdown PDAC. In prostate cancer, a reduction in Mic60 levels is associated with multiple cellular stress signals (20). This includes the upregulation of a senescence-associated secretory phenotype (SASP), a transcriptional inflammatory response often associated with mitochondrial dysfunction (36) that impairs tumor cell proliferation (20). Mic60 depletion in PDAC did not involve a SASP but upregulated stress-associated protein targets of TNFα-NFκB signaling implicated in cell death and cell survival (5), BIRC3, BIRC2, FAS, BCL2A1, CASP1, core components of autophagy, BECN1, ATG5, ATG12, and mediators of apoptosis, BAX, CASP7, APAF1 (Fig. 4*A* and *SI Appendix*, Fig. S6*A*). In addition, Mic60-knockdown PDAC cells activated multiple receptor tyrosine kinase (RTK)/growth factor receptor networks in a phospho-protein array (Fig. 4*B* and *SI Appendix*, Fig. S6*B*). This included regulators of cell proliferation (FGFR1, ErbB2, PDGF-R), angiogenesis (VEGFR, Tie-2, Eph), and tumor cell motility (DDR1, TrkC) (Fig. 4*B* and *SI Appendix*, Fig. S6*B*), previously implicated in PDAC progression, aberrant cell survival, and poor outcome (37, 38).

To test how the activation of these proliferative signals may affect Mic60-knockdown PDAC growth, we first stably expressed pLKO or shMic60 in murine cell lines, 2838c3 and 6419c5 isolated from a KPC genetic model of pancreatic cancer (K-rasLSL.G12D/+;Trp53R172H/+;Pdx-1-Cre) (*SI Appendix*, Fig. S6*C*). We found that Mic60-knockdown 6419c5 cells exhibited faster cell cycle progression as quantified by CellTrace analysis and flow cytometry (Fig. 4*C* and *SI Appendix*, Fig. S6*D*) and accelerated tumor growth when engrafted in syngeneic C57BL/6J mice (Fig. 4*D*). Similar results were obtained with human PANC-1 cells, where reduction in Mic60 levels was associated with increased cell proliferation, compared to controls (*SI Appendix*, Fig. S6*E*).

Preclinical Targeting of Mitochondrial dsRNA in PDAC. The results above suggest that Mic60-knockdown PDAC exploits mitochondrial NFκB inflammation (5) and the activation of compensatory gene expression networks to buffer cellular *stress*, and maintain tumor growth (20). To begin testing this possibility in initial proof-of-concept experiments, we treated control or Mic60-knockdown PDAC cells with pXSC, a small molecule inhibitor of p50 NFκB DNA binding. Within minutes of exposure, pXSC caused complete but selective cell death (Fig. 4*E* and Movie S1), killing Mic60-knockdown PDAC cells at IC_{50} concentrations ~1,000-fold lower than control cultures (Fig. 4*E*). As an independent approach, we used a neutralizing monoclonal antibody, XT3.11 to directly target TNFα in this pathway, which has been implicated in PDAC growth (39). Incubation with XT3.11 dose-dependently killed PDAC cells after Mic60 depletion by siRNA (Fig. 4 *F*, *Left*) or stable shRNA (Fig. 4 *F*, *Right*) expression, whereas parental PANC-1 cells were not affected (Fig. 4*F*).

These responses were specific because exposure to the chemotherapeutic agent, gemcitabine, a standard of care for PDAC patients (*SI Appendix*, Fig. S7*A*), or serum deprivation (*SI Appendix*, Fig. S7*B*), killed PDAC cells, irrespective of Mic60 levels. Consistent with these results, systemic administration of XT3.11 antibody selectively inhibited the growth of Mic60-knockdown 6419c5 tumors, whereas control tumors were not affected (Fig. 4 *G* and *H*). Histologically, anti-TNFα therapy disrupted the glandular architecture of Mic60-knockdown KPC tumors, with formation of large areas of tissue necrosis (Fig. 4*I*). Conversely, no histological changes were observed in pLKO-expressing 6419c5 KPC tumors with or without anti-TNFα treatment (Fig. 4*I*).

We next looked at the cell death mechanisms activated by targeting NFκB in Mic60-knockdown PDAC. We found that a small molecule inhibitor of the necrosome complex, necrostatin-1 (NEC1) reversed the cytotoxic effect of pXSC and preserved the viability of Mic60-knockdown PDAC cells (*SI Appendix*, Fig. S7*C* and Movie S2). Similar results were obtained after siRNA depletion of the necrosome-associated RIP1 kinase, which preserved tumor cell viability in the presence of pXSC (*SI Appendix*, Fig. S7*D*). In contrast, z-VAD-fmk, a broad-spectrum caspase inhibitor and suppressor of apoptosis, had no effect (*SI Appendix*, Fig. S7*C* and Movie S3). Collectively, these data suggest that targeting NFκB signaling potently activates necroptosis in PDAC, a form of inflammatory cell death (40), regulated by multiple NFκB checkpoints (41).

Although a key tumor driver, targeting NFκB for cancer therapy is challenging. Conversely, the TLR3–TRAF6 signaling pathway (27, 28) is druggable by small molecule modulators (42). The role of TLR3 in cancer is debated (42), linked to both tumor stimulatory and inhibitory effects (33). In the TCGA dataset, PDAC patients exhibited higher levels of TLR3, compared to normal pancreas (*SI Appendix*, Fig. S7*E*). By bioinformatics analysis, this

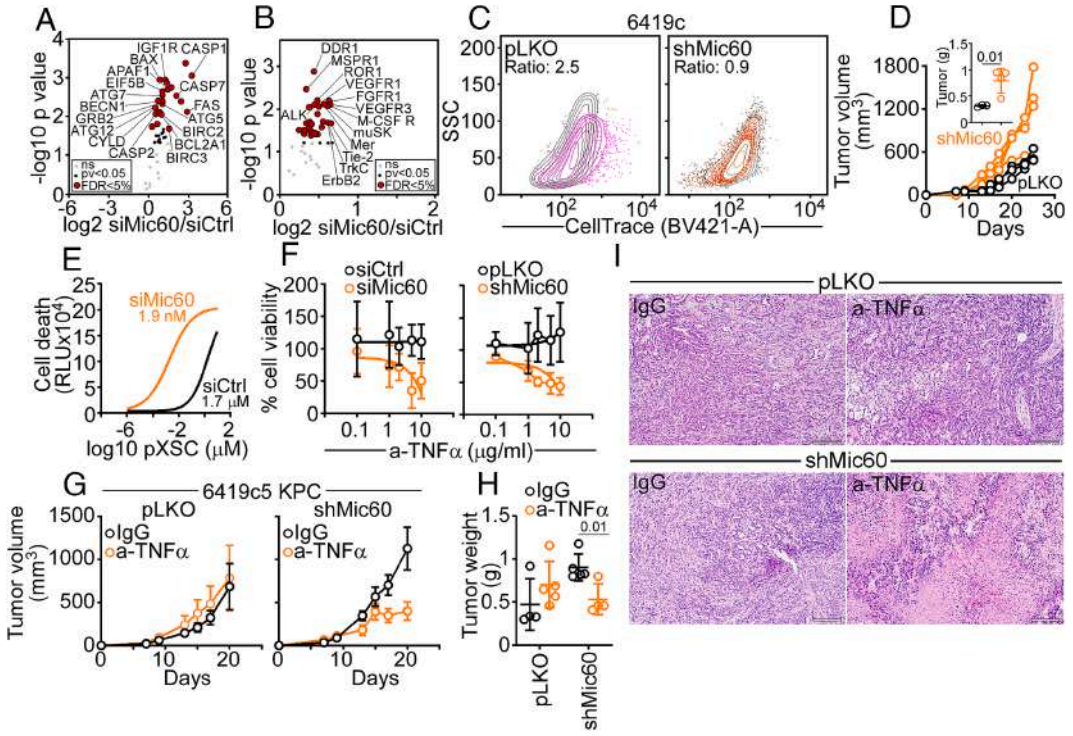

Fig. 4. Mitochondrial inflammation maintains PDAC growth. (*A*) PANC-1 cells expressing siCtrl or siMic60 were profiled in a cell death pathway array by RT-qPCR. Data are expressed as a volcano plot of log2 ratios between the groups (FDR < 5%, $P < 0.05$). (*B*) PANC-1 cells as in (*A*) were analyzed in a receptor tyrosine kinase (RTK) phosphoprotein array. Data are expressed as a volcano plot of log2 ratios of protein spots between the two groups quantified by densitometry (two independent replicates). (*C*) KPC-derived 6419c5 murine pancreatic cancer cells stably expressing pLKO or shMic60 were stained with CellTrace and analyzed for differences in cell proliferation by flow cytometry. Data are expressed as density plots of ratios of fluorescence intensity between unstained (black tracing) and stained cells on day 7 of culture. Purple tracing, pLKO; orange tracing, shMic60. (*D*) KPC 6419c5 cells as in (*C*) were engrafted onto the flank of syngeneic C57BL/6J mice and tumor growth was measured with a caliper at the indicated time intervals. *Inset*, tumor weight at day 26. (*E*) PANC-1 cells expressing siCtrl or siMic60 were incubated with increasing concentration of small molecule NFκB inhibitor, pXSC and analyzed for cell death by chemiluminescence. The IC_{50} concentrations are indicated. (*F*) PANC-1 cells expressing siCtrl or siMic60 (*Left*) or pLKO or shMic60 (*Right*) were incubated with increasing concentrations of a neutralizing antibody to TNFα (a-TNFα, XT3.11) and analyzed for cell viability by direct cell counting. Mean±SD (n = 3). (*G*) C57BL/6J mice engrafted with murine KPC 6419c5 cells expressing pLKO or shMic60 were treated with IgG or a-TNFα XT3.11 antibody (10 mg/kg i.p. 3 times per week) and examined for tumor growth at the indicated time intervals. (*H*) The conditions are as in (*G*) and tumor weight on day 20 was quantified in the individual groups. Each symbol corresponds to a single mouse determination. Numbers are *P* values by two-tailed unpaired *t* test. (*I*) KPC 6419c5 tumors as in (*G*) were analyzed histologically by hematoxylin-eosin staining. Representative images. (Scale bar, 100 μm.)

was associated with heightened IFN gene expression (*SI Appendix*, Fig. S7*F*) and upregulation of a Mic60-knockdown inflammatory transcriptome (*SI Appendix*, Fig. S7*G*), whereas Myc target genes were suppressed (*SI Appendix*, Fig. S7*H*). Differences in patient survival based on TLR3 levels did not reach statistical significance ($TLR3^{high}$, n = 55; $TLR3^{low}$, n = 115; $P = 0.08$).

Against this backdrop, treatment with TRAF6i selectively killed Mic60-knockdown human (PANC-1) (Fig. 5*A*) or murine (6419c5) (Fig. 5*B*) pancreatic cancer cells, compared to controls. In addition, systemic administration of TRAF6i suppressed the growth of Mic60-knockdown 6419c5 KPC tumors in syngeneic mice, whereas tumors generated by 6419c5 cells expressing pLKO were not affected (Fig. 5*C*). TRAF6i therapy was well tolerated and did not result in animal weight loss throughout treatment (Fig. 5*D*).

We next asked if this antitumor response required an intact immune system, and we grew 6419c5 tumors in immunocompromised NSG mice. Systemic TRAF6i therapy was equally effective in these settings, selectively blocking the growth of Mic60-knockdown 6419c5 KPC tumors, but not KPC tumors expressing pLKO (Fig. 5*E*). TRAF6i administration was safe also in the absence of an immune system, with no significant animal weight loss throughout treatment (Fig. 5*F*). By IHC, KPC tumors expressed high levels of TRAF6, consistent with pathway activation, in vivo (Fig. 5*G*).

In summary, we have shown that PDAC, and potentially other malignancies, exploit antiviral signaling that protects against invading pathogens to stimulate chronic inflammation, reprogram transcriptional networks of cell proliferation and cell survival and fuel tumor growth, in vivo. Far from promoting antitumor immunity (43), chronic inflammation and sustained IFN signaling are linked to immunosuppression (44), a common finding in PDAC (45), via CD8 T cell "exhaustion" (46), loss of effector functions (47) and accumulation of immunosuppressive cellular subsets in the microenvironment (45). Mechanistically, and different from previous examples of viral mimicry (7), this inflammatory pathway originates in mitochondria, where loss of organelle integrity due to reduced levels of Mic60 (20), causes the release of dsRNA normally generated during mitochondrial DNA transcription. In turn, the released dsRNA engages multiple *sensors*, in particular, cytosolic RIG-I (29) and endosomal TLR3–TRAF6 (27, 28) to drive NFκB gene expression, IFN production, and cytokine release. There is also precedent for extracellular release of mitochondrial dsRNA and uptake by neighboring cells (16), which may explain the contribution of endosomal TLR3 in this pathway.

Despite the activation of multiple compensatory gene expression networks of cell proliferation, Mic60-knockdown PDAC cells remain uniquely dependent, or "addicted" to NFκB signaling, consistent with its role as a nearly universal tumor driver (5). In turn, this creates an actionable therapeutic vulnerability, and genetic or pharmacologic targeting of TLR3–TRAF6 signaling selectively killed Mic60-knockdown tumor cells and suppressed

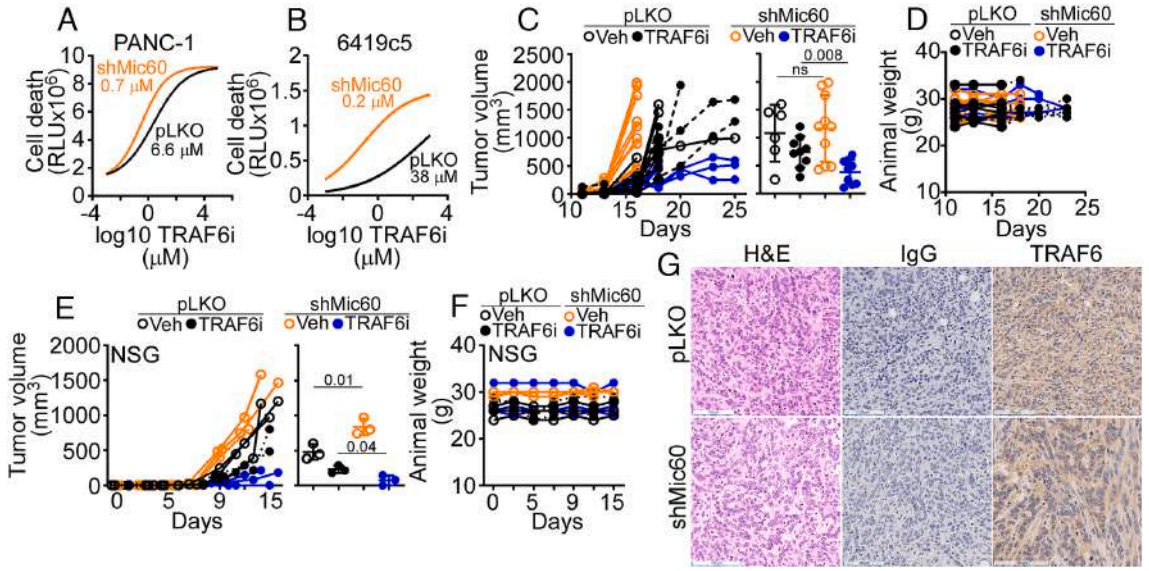

Fig. 5. Preclinical targeting of TRAF6 inflammation in PDAC. (*A* and *B*) PANC-1 (*A*) or KPC 6419c5 (*B*) cells stably expressing pLKO or shMic60 were treated with the indicated increasing concentrations of small molecule TRAF6 inhibitor (TRAF6i) and analyzed for cell death by chemiluminescence. The IC_{50} concentrations are indicated. (*C*) KPC 6419c5 cells as in (*B*) were engrafted onto the flanks of syngeneic C57BL/6J mice, treated i.p. with vehicle (Veh) or TRAF6i (1 μg/kg in 30 μL daily i.p.) when tumors reached ~120 mm^3 and tumor growth was quantified with a caliper at the indicated time intervals (*Left*). *Right*, average tumor volumes at day 20. (*D*) The conditions are as in (*C*) and animal weight was quantified in each group at the indicated time intervals. (*E*) Immunocompromised NSG mice were engrafted with KPC 6419c5 cells expressing pLKO or shMic60, treated with vehicle or TRAF6i (1 μg/kg daily i.p.) and tumor growth was quantified at the indicated time intervals with a caliper (*Left*). *Right*, average tumor volumes at day 18. (*F*) The conditions are as in (*E*) and changes in animal weight were quantified at the indicated time intervals during TRAF6i treatment. (*G*) KPC 6419c5 tumors as in (*C*) were analyzed for TRAF6 expression by immunohistochemistry. Representative images. (Scale bar, 100 μm.) For panels *C*–*F*, each symbol corresponds to a single mouse determination. Numbers are *P* values by the two-tailed unpaired *t* test.

PDAC growth in preclinical models, without overt systemic toxicity. Prior attempts to block TNFα-NFκB signaling in unselected PDAC patients (39) did not produce clinical gains (48). The results here suggest that TRAF6 inhibition may provide benefit in preselected, Mic60-low PDAC patients, shutting off NFκB cell survival, lowering protumorigenic inflammation (30), and blocking immunosuppressive reprogramming of the microenvironment (49).

Materials and Methods

Patients. All patient-related research described in this study was approved by the Institutional Review Board (IRB) of Christiana Care Health System (Newark, DE) where the pancreas tissue investigated in this study is procured. The consent contents for tissue collection, including a statement that the study involves research, an explanation of the purpose of the research, a statement that participation is voluntary and that refusal to participate will involve no penalty or loss of benefits to which the patient is otherwise entitled, are discussed by the surgeon performing the procedure at Christiana Care with a witness in the office prior to the surgery. The consents are IRB approved and all physicians who participate in research complete the necessary Collaborative Institutional Training Initiative Program (CITI) of human subjects.

Pancreas tissue samples harvested from ten patients with histologically confirmed diagnosis of locally invasive pancreatic ductal adenocarcinoma (PDAC) age 44 to 94 y of age (*SI Appendix*, Table S1) were immediately placed on dry ice upon surgical collection and stored at −80 °C until use. Tissue samples were processed for RNA extraction, immunoprecipitation with antibody J2 to dsRNA and sequence alignment of immune complexes with the mitochondrial genome. In some experiments, formalin-fixed, paraffin-embedded pancreas tissue sections from the same PDAC patient cohort were processed by immunohistochemistry. A cohort of nonsmall cell lung cancer (NSCLC) patients with surgically resected metastases to the brain has been described (26).

Immunoprecipitation and Sequencing of dsRNA. Protein G Dynabeads (ThermoFisher Scientific) were washed and suspended in a RNA lysis buffer (Zymo). Five μg of J2 antibody were bound to 100 μL of beads for 1 h at 22 °C and conjugated beads were washed with RNA lysis Buffer. PANC-1 cells (80% confluency) were washed with 10 mL of ice-cold DPBS, scraped and centrifuged at 500 × *g* for 5 min at 4 °C. The cell pellet was lysed with 1 mL of RNA lysis buffer incubated on ice for 5 min and centrifuged at 17,000 × *g* for 5 min at 4 °C. Total RNA was harvested from 10% input lysate using Trizol reagent. For immunoprecipitation, 1 mL aliquots of PANC-1 lysate were mixed with 10 U RNase free TurboDNase (Ambion) in 10 mM $MgCl_2$ per 1 mL of mix and further incubated with 100 μL of J2-Dynabeads for 4 h at 4 °C. After magnetic separation, beads were washed twice with 1 mL of high salt washing buffer (HSWB) containing 50 mM Tris-Cl, pH 7.4, 1 M NaCl, 1 mM EDTA, 1% NP-40, 0.5% DOC, 0.1% SDS, transferred to a new tube containing NET-2 buffer and washed twice. J2-bound dsRNA was extracted with Trizol reagent and sequenced. cDNA libraries were generated using the NEBNext Ultra II Directional RNA library Prep Kit (New England Biolabs) and subsequently sequenced on an Illumina HiSeq-2000 with 100-bp paired end reads.

Bioinformatics Analysis. To evaluate the prognostic significance of a 7-gene panel representative of Mic60-knockdown gene signature (EIF2AK2, TLR3, OAS1, MX1, CASP1, NUFIP2, and PPIA) in PDAC, we utilized the publicly available Pancreatic Adenocarcinoma (PAAD) dataset from The Cancer Genome Atlas (TCGA). From the PAAD dataset, we selected only diagnostic samples, excluding neuroendocrine carcinoma cases, resulting in 170 patient samples for subsequent analysis. To derive a unified measure of gene set expression, we employed gene set variation analysis (GSVA), specifically using single-sample gene set enrichment analysis (ssGSEA), as implemented in the GSVA R package (50). GSVA transforms the gene-by-sample expression matrix into a gene-set-by-sample expression score, effectively summarizing the collective expression of the selected seven genes across individual samples. A waterfall plot was generated to visualize the distribution of these gene set scores across the patient cohort. Next, patients were stratified into low- and high-expression groups (54 and 116, respectively) based on an optimal cutoff point for the continuous gene set scores, determined using the cutp function from the survMisc R package (51). Kaplan–Meier survival analysis, supplemented by a Cox proportional hazards model, was then conducted to compare overall survival (OS) between the low- and high-expression groups.

TCGA RNA-seq data were downloaded from UCSC Xena (52) "TCGA Pan-Cancer (PANCAN)" data hub processed by "TOIL RSEM fpkm" pipeline in a form of log2 (fpkm + 0.001) values and converted to absolute FPKM values. Mitochondrial content was calculated as a sum of FPKM values for mitochondrial genes divided by total FPKM sum.

Data, Materials, and Software Availability. All study data are included in the article and/or supporting information.

ACKNOWLEDGMENTS. This work was supported by NIH Grants R35 CA220446 (D.C.A.), R50 CA221838 (H.-Y.T.), and R50 CA211199 (A.V.K.). M.Y. is supported by a Cotswold Foundation Postdoctoral Fellowship. Wistar Shared Resources are supported by P30 CA010815. We thank Dr. Ben Stanger (University of Pennsylvania) for generously providing KPCY 6419c5 cells.

Author affiliations: [a]Genome Regulation and Cell Signaling Program, The Wistar Institute, Philadelphia, PA 19104; [b]Department of Pharmacy, School of Medicine and Surgery, University of Naples Federico II, Naples 80138, Italy; [c]Bioinformatics Shared Resource, The Wistar Institute, Philadelphia, PA 19104; [d]Proteomics Shared Resource, The Wistar Institute, Philadelphia, PA 19104; [e]Molecular and Cellular Oncogenesis Program, The Wistar Institute, Philadelphia, PA 19104; [f]Department of Pathophysiology and Transplantation, University of Milan, Milan 20122, Italy; [g]Division of Pathology, Fondazione Istituto di Ricovero e Cura a Carattere Scientifico Ca' Granda-Ospedale Maggiore, Milano 20122, Italy; [h]Division of Thoracic Surgery and Lung Transplantation, Fondazione Istituto di Ricovero e Cura a Carattere Scientifico Ca' Granda-Ospedale Maggiore Policlinico, Milano 20122, Italy; [i]Division of Neurosurgery, Fondazione Istituto di Ricovero e Cura a Carattere Scientifico Ca' Granda-Ospedale Maggiore Policlinico, Milano 20122, Italy; [j]Department of Pathology, Helen F. Graham Cancer Center and Research Institute, Christiana Care Health, Newark, DE 19713; [k]Helen F. Graham Cancer Center and Research Institute, Christiana Care Health, Newark, DE 19713; and [l]Division of Surgical Oncology, Helen F. Graham Cancer Center and Research Institute, Christiana Care Health, Newark, DE 19713

Author contributions: N.J.P. and D.C.A. designed research; A.T.M., M.Y., C.E., P.K., A.V.K., J.M., A.M.F., H.-Y.T., A.M.S., V.V., M.V.I., A.W., and M.P. performed research; A.P., M.L., V.V., M.V.I., A.S., and N.J.P. contributed new reagents/analytic tools; A.V.K., J.M., A.M.F., H.-Y.T., A.M.S., A.P., M.L., V.V., M.V.I., N.J.P., M.P., and D.C.A. analyzed data; and M.P. and D.C.A. wrote the paper.

1. M. M. Mehta, S. E. Weinberg, N. S. Chandel, Mitochondrial control of immunity: Beyond ATP. *Nat. Rev. Immunol.* **17**, 608–620 (2017).
2. E. L. Mills, B. Kelly, L. A. J. O'Neill, Mitochondria are the powerhouses of immunity. *Nat. Immunol.* **18**, 488–498 (2017).
3. M. Dong, K. A. Fitzgerald, DNA-sensing pathways in health, autoinflammatory and autoimmune diseases. *Nat. Immunol.* **25**, 2001–2014 (2024).
4. S. M. Belgnaoui, S. Paz, J. Hiscott, Orchestrating the interferon antiviral response through the mitochondrial antiviral signaling (MAVS) adapter. *Curr. Opin. Immunol.* **23**, 564–572 (2011).
5. K. Taniguchi, M. Karin, NF-kappaB, inflammation, immunity and cancer: Coming of age. *Nat. Rev. Immunol.* **18**, 309–324 (2018).
6. L. M. Snell, T. L. McGaha, D. G. Brooks, Type i interferon in chronic virus infection and cancer. *Trends Immunol.* **38**, 542–557 (2017).
7. M. Schlee, G. Hartmann, Discriminating self from non-self in nucleic acid sensing. *Nat. Rev. Immunol.* **16**, 566–580 (2016).
8. D. Roulois *et al.*, DNA-demethylating agents target colorectal cancer cells by inducing viral mimicry by endogenous transcripts. *Cell* **162**, 961–973 (2015).
9. G. Deblois *et al.*, Epigenetic switch-induced viral mimicry evasion in chemotherapy-resistant breast cancer. *Cancer Discov.* **10**, 1312–1329 (2020).
10. N. Sasaki *et al.*, RNA sensing induced by chromosome missegregation augments anti-tumor immunity. *Mol. Cell* **85**, 770–786.e777 (2025).
11. E. A. Bowling *et al.*, Spliceosome-targeted therapies trigger an antiviral immune response in triple-negative breast cancer. *Cell* **184**, 384–403.e321 (2021).
12. K. B. Chiappinelli *et al.*, Inhibiting DNA methylation causes an interferon response in cancer via dsRNA including endogenous retroviruses. *Cell* **162**, 974–986 (2015).
13. A. P. West *et al.*, Mitochondrial DNA stress primes the antiviral innate immune response. *Nature* **520**, 553–557 (2015).
14. A. Dhir *et al.*, Mitochondrial double-stranded RNA triggers antiviral signalling in humans. *Nature* **560**, 238–242 (2018).
15. R. Chen, C. A. Ishak, D. D. De Carvalho, Endogenous retroelements and the viral mimicry response in cancer therapy and cellular homeostasis. *Cancer Discov.* **11**, 2707–2725 (2021).
16. S. Kim *et al.*, Mitochondrial double-stranded RNAs govern the stress response in chondrocytes to promote osteoarthritis development. *Cell Rep.* **40**, 111178 (2022).
17. V. Lopez-Polo *et al.*, Release of mitochondrial dsRNA into the cytosol is a key driver of the inflammatory phenotype of senescent cells. *Nat. Commun.* **15**, 7378 (2024).
18. S. Srinivasan, M. Guha, A. Kashina, N. G. Avadhani, Mitochondrial dysfunction and mitochondrial dynamics–The cancer connection. *Biochim. Biophys. Acta: Bioenerg.* **1858**, 602–614 (2017).
19. M. van der Laan, S. E. Horvath, N. Pfanner, Mitochondrial contact site and cristae organizing system. *Curr. Opin. Cell Biol.* **41**, 33–42 (2016).
20. J. C. Ghosh *et al.*, Ghost mitochondria drive metastasis through adaptive GCN2/Akt therapeutic vulnerability. *Proc. Natl. Acad. Sci. U.S.A.* **119**, e2115624119 (2022).
21. A. V. Kossenkov *et al.*, Mitochondrial fitness and cancer risk. *PLoS ONE* **17**, e0273520 (2022).
22. W. Park, A. Chawla, E. M. O'Reilly, Pancreatic cancer: A review. *JAMA* **326**, 851–862 (2021).
23. C. J. Halbrook, C. A. Lyssiotis, M. Pasca di Magliano, A. Maitra, Pancreatic cancer: Advances and challenges. *Cell* **186**, 1729–1754 (2023).
24. A. N. Hosein, R. A. Brekken, A. Maitra, Pancreatic cancer stroma: An update on therapeutic targeting strategies. *Nat. Rev. Gastroenterol. Hepatol.* **17**, 487–505 (2020).
25. F. Weber, V. Wagner, S. B. Rasmussen, R. Hartmann, S. R. Paludan, Double-stranded RNA is produced by positive-strand RNA viruses and DNA viruses but not in detectable amounts by negative-strand RNA viruses. *J. Virol.* **80**, 5059–5064 (2006).
26. A. Morotti *et al.*, Epigenetic rewiring of metastatic cancer to the brain: Focus on lung and colon cancers. *Cancers (Basel)* **15**, 2145 (2023).
27. S. Y. Zhang *et al.*, TLR3 immunity to infection in mice and humans. *Curr. Opin. Immunol.* **25**, 19–33 (2013).
28. L. Alexopoulou, A. C. Holt, R. Medzhitov, R. A. Flavell, Recognition of double-stranded RNA and activation of NF-kappaB by toll-like receptor 3. *Nature* **413**, 732–738 (2001).
29. M. van Huizen, M. U. Gack, The RIG-I-like receptor family of immune proteins. *Mol. Cell* **85**, 3793–3806 (2025).
30. D. T. Starczynowski *et al.*, TRAF6 is an amplified oncogene bridging the RAS and NF-κB pathways in human lung cancer. *J. Clin. Invest.* **121**, 4095–4105 (2011).
31. K. A. Cottrell, R. J. Andrews, B. L. Bass, The competitive landscape of the dsRNA world. *Mol. Cell* **84**, 107–119 (2024).
32. E. Latz *et al.*, TLR9 signals after translocating from the ER to CpG DNA in the lysosome. *Nat. Immunol.* **5**, 190–198 (2004).
33. N. J. Gay, M. Gangloff, A. N. Weber, Toll-like receptors as molecular switches. *Nat. Rev. Immunol.* **6**, 693–698 (2006).
34. H. Ishikawa, Z. Ma, G. N. Barber, STING regulates intracellular DNA-mediated, type I interferon-dependent innate immunity. *Nature* **461**, 788–792 (2009).
35. P. G. Thomas *et al.*, The intracellular sensor NLRP3 mediates key innate and healing responses to influenza A virus via the regulation of caspase-1. *Immunity* **30**, 566–575 (2009).
36. C. D. Wiley *et al.*, Mitochondrial dysfunction induces senescence with a distinct secretory phenotype. *Cell Metab.* **23**, 303–314 (2016).
37. S. J. Coleman *et al.*, Nuclear translocation of FGFR1 and FGF2 in pancreatic stellate cells facilitates pancreatic cancer cell invasion. *EMBO Mol. Med.* **6**, 467–481 (2014).
38. J. Taeger *et al.*, Targeting FGFR/PDGFR/VEGFR impairs tumor growth, angiogenesis, and metastasis by effects on tumor cells, endothelial cells, and pericytes in pancreatic cancer. *Mol. Cancer Ther.* **10**, 2157–2167 (2011).
39. M. S. Alam *et al.*, TNFR1 signaling promotes pancreatic tumor growth by limiting dendritic cell number and function. *Cell Rep. Med.* **5**, 101696 (2024).
40. Y. S. Cho *et al.*, Phosphorylation-driven assembly of the RIP1-RIP3 complex regulates programmed necrosis and virus-induced inflammation. *Cell* **137**, 1112–1123 (2009).
41. Y. Dondelinger *et al.*, NF-kappaB-independent role of IKKalpha/IKKbeta in preventing RIPK1 kinase-dependent apoptotic and necroptotic cell death during TNF signaling. *Mol. Cell* **60**, 63–76 (2015).
42. M. L. Hsieh, D. Nishizaki, J. J. Adashek, S. Kato, R. Kurzrock, Toll-like receptor 3: A double-edged sword. *Biomark. Res.* **13**, 32 (2025).
43. G. M. Boukhaled, S. Harding, D. G. Brooks, Opposing roles of type I interferons in cancer immunity. *Annu. Rev. Pathol.* **16**, 167–198 (2021).
44. J. L. Benci *et al.*, Tumor interferon signaling regulates a multigenic resistance program to immune checkpoint blockade. *Cell* **167**, 1540–1554.e1512 (2016).
45. T. Tang *et al.*, Transcriptional control of pancreatic cancer immunosuppression by metabolic enzyme CD73 in a tumor-autonomous and -autocrine manner. *Nat. Commun.* **14**, 3364 (2023).
46. L. M. McLane, M. S. Abdel-Hakeem, E. J. Wherry, CD8 T cell exhaustion during chronic viral infection and cancer. *Annu. Rev. Immunol.* **37**, 457–495 (2019).
47. C. U. Blank *et al.*, Defining "T cell exhaustion". *Nat. Rev. Immunol.* **19**, 665–674 (2019).
48. C. Wu *et al.*, Disrupting cytokine signaling in pancreatic cancer: A phase I/II study of etanercept in combination with gemcitabine in patients with advanced disease. *Pancreas* **42**, 813–818 (2013).
49. M. Liu *et al.*, The crosstalk between macrophages and cancer cells potentiates pancreatic cancer cachexia. *Cancer Cell* **42**, 885–903.e884 (2024).
50. S. Hanzelmann, R. Castelo, J. Guinney, GSVA: Gene set variation analysis for microarray and RNA-seq data. *BMC Bioinf.* **14**, 7 (2013).
51. C. Dardis, survMisc: Miscellaneous functions for survival data (R Package Version 0.5.6, Comprehensive R Archive Network (CRAN), Vienna, Austria, 2016). https://CRAN.R-project.org.
52. M. J. Goldman *et al.*, Visualizing and interpreting cancer genomics data via the Xena platform. *Nat. Biotechnol.* **38**, 675–678 (2020).